Lateral Plastic Collapse of Cylinders: Experiments and Modeling

K. Nesnas[1] and A. Abdul-Latif[2]

Abstract: Large plastic collapse of an identical pair of cylinders of various geometries having the same length and volume is studied under lateral compressive load. Superplastic material is employed as a representative material to simulate the classical engineering material behavior under high strain rate. The effects of the strain rate and the geometry of cylinders on the plastic collapse are taken into account. The experimental study is conducted using a structure in which one cylinder is superplastic and the other is steel (referred to as deformable and non-deformable situation "DND"). The actual structure (DND) and that one investigated experimentally by Abdul-Latif (2000) are modeled. This latter is referred to as "deformable situation". A standard numerical study is conducted based on the updated Lagrangian formulation starting from the principle of virtual power. The inelastic flow is described by a simple power law of Norton-Hoff type. It is demonstrated that the predictions describe fairly well the available experimental results.

keyword: large deformation, energy dissipating system, strain rate effect, superplastic material, non-linear finite element.

1 Introduction

The problem of large plastic strain of circular tubes subjected to transverse compressive load has been the subject of extensive experimental and theoretical researches over the past three decades. One of the most important engineering application is the energy dissipating systems. Such an application has a substantial role in mit-

[1] GSM/LASMIS, Université de Technologie de Troyes,
B.P. 2060, 10010
Troyes cedex, France
[2] Corresponding author.
ERBEM/GIM, Université Paris
8, IUT de Tremblay, 93290
Tremblay-en-France, France
Tel.: (33) 1-41-51-12-34;
Fax: (33) 1-48-61-38-17;
e-mail:aabdul@iut-tremblay.univ-paris8.fr

igating the damage and thus improving the crashworthiness and vehicular collisions [for example, Ezra and Fay (1972); Rawlings (1974); Johnson and Ried (1978 and 1986); Jones (1989)]. Because of the widespread use of the tubular components in these systems, a focusing is made here on such elements. In the context of energy dissipating system, the plastic flattening of cylinders due to lateral compressive force represents a device having a good efficiency to absorb energy. Moreover, it has a desirable characteristic concerning the smooth load-deflection relation. These tubes are also easier to build than most other devices [DeRutz and Hodge (1963); Rewood (1964); Johnson, Reid and Reddy (1977); Reid and Reddy (1978); Reddy and Reid (1979); Reid and Reddy (1979); and others].

The superplasticity can be defined as large neck-free extensions. This material shows low strength and high elongation of the order of 1000 per cent before fracture in some cases and is highly strain-rate sensitive [Johnson and Mellor (1975)]. The two principal classes of superplastic process are (a) transformation plasticity occurring during a phase change as in steels; (b) micrograin plasticity: its distinguishing feature being the stability and finesse of the microstructure as in a tin-lead alloy. The superplastic tin-lead alloy can satisfactorily be used under quasi-static condition to simulate the metallic engineering materials under dynamic loading as shown by Abdul-Latif (2000). However, in many cases, the mode of deformation under dynamic loading is different from that under quasi-static one. This is due to the inertia forces particularly when elastic and plastic stress wave effects dominate, or when thermoplastic phenomenon occurs [Johnson (1972)].

The finite element analysis is desirable and interesting. In the past two decades, many research efforts have been expended to develop analysis capabilities for large plastic strain problems with contact friction. In fact, Signorini (1959) initiated the variational theory of contact mechanics. Based on Lagrange multiplier method or the penalty-function scheme, finite element analysis has been studied

by Oden and Kikuchi (1982), Oden and Carey (1984) and Cheng and Kikuchi (1985). To model the contact with friction, an algorithm is presented in Pasquinelli (1995), where a direct application and control of boundary conditions are used to deal with the friction conditions. The proceeding of NUMIFORM'92 [Chenot, Wood and Zienkiewicz (1992)] presents several recent developments in this field. The posed boundary value problem involves the coupling between geometrical and material non-linearities in the case of large deformation with contact friction aspect.

In this work, the NLFE method is used to model the lateral collapse of two geometrically identical cylinders of various inside/outside diameter ratios (R= di/do) ranging from 0 to 0.473. Numerical solutions are carried out in finite rate-dependent plasticity (viscoplasticty) adopting the assumptions of plane strain and Norton-Hoff's law as material behavior. Two different structural situations are studied. In the first case, both cylinders are made from superplastic material (deformable situation), while in the second case, one cylinder is superplastic and the other is steel (DND). The steel cylinder deforms, in this case, elastically during the test, whereas the superplastic cylinder deforms plastically. These different situations and geometries are tested under different strain rates in the range of 10^{-5}/s to 10^{-3}/s. The NLFE technique can appropriately reproduce the observed plastic flow, the compressive force and the energy absorbed evolution during the plastic collapse of cylinders under different strain rates. It is noteworthy that the novelty of this work is related to the types of the energy absorber device and its experimental finding as well as the numerical results which are performed with a simple constitutive law. In fact, the numerical simulation is performed with a commercial finite element code FORGE2. This leads, despite its simplicity, to well describe the collapse behavior of the several cylindrical geometries under transverse loadings with different strain rates.

2 Experimental Procedure and Results

Cylindrical specimens, either solid or hollow, of different di/do (R) values made from superplastic tin-lead (61.9% - 38.1% by weight) alloy were produced by forward extrusion with about 80% reduction. As all these different right circular specimens have almost the same cross-sectional area, hence, the initial billet size of 56 mm diameter is always used to produce these cylinders. The ex-

truded specimen lengths are of 120 mm. From each end of cylinder, a length of 20 mm is always discarded after extrusion. All the hollow cylinders are produced using different bore of extrusion cylinders and different diameter mandrels. In the case of hollow cylinder production, the initial billets have to be drilled, before achieving the extrusion process, according to the mandrel's diameter value. The reduction ratio, in the solid case (di/do = 0), is of 81% , while in the second extremity case (di/do = 0.473), the reduction represents 80% . Thus, the maximum deviation can not exceed 1% giving rise practically, as it is assumed, to the same material properties. The final dimensions of the employed cylinders are listed in Table 1. The experimental tests are conducted using a special rig (Fig.1). This rig consists of a steel frame,
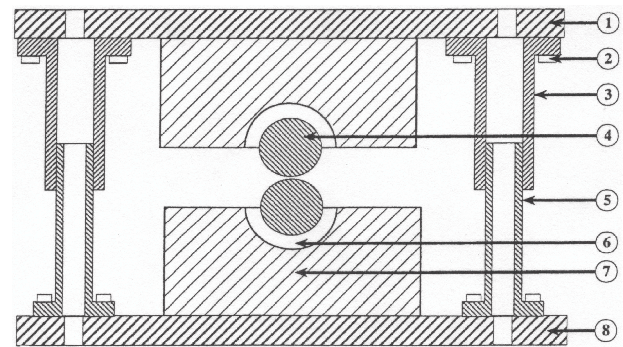
1: upper platen   2: screw   3: bush
4: specimen   5: guide   6: specimen
7: base   8: lower platen   accommodator
Figure 1 : Sectioned view of the employed rig.

which holds and locates two thick semi-cylindrical parts that accommodate and hold in position the cylinders to be tested. All the experimental tests are loaded between the platens of an Instron Universal Testing Machine at three constant cross head speeds, namely 0.2, 5, and 20 mm/min, giving representative strain rates of 7×10^{-5}/s, 1.8×10^{-3}/s and 7×10^{-3}/s, respectively. For further details about the strain rates determination, the reader is to refer to the [Abdul-Latif (2000)]. In order to ensure the experimental results accuracy, each test was repeated twice under the same experimental conditions (applied speed and temperature). The tests are always conducted at room temperature. If the difference between the two responses exceeds 3% , then another test has to be performed. For each case of R, three tests are conducted under increasing loading at different strain rates given

above. Figs. 2a, b, c and d show some selected load-deflection behaviors in the case of R= 0, 0.283, 0.348 and 0.473 respectively for DND situation.

In order to study the flow mechanism in the case of DND, the collapsed cylinders were sectioned, polished, projected on a profile projector at a magnification of ten and then traced. Fig. 3 shows traces of cross sections of a cylinder having di/do (0.348) which was deformed to two axial displacements 6 and 10 mm.
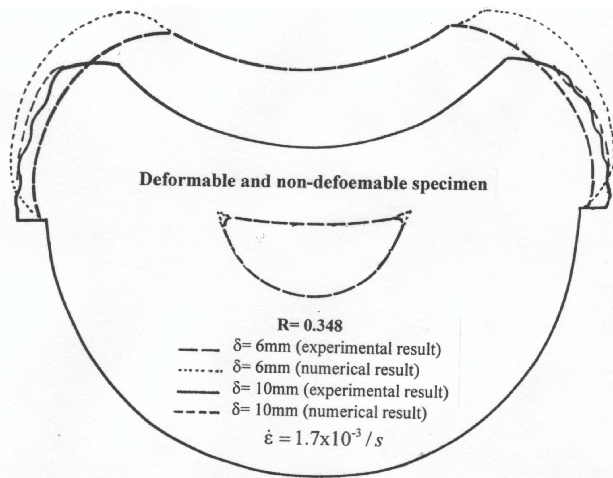

Figure 3 : Profiles of projected cross sections of hollow cylinders at di/do=0.348 after deformation in the deformable and non-deformable situation (numerical and experimental comparison).

Experimentally, the variation of the energy absorbed per unit volume with di/do ratio is pointed out in Fig. 4a and 4b for axial displacements 4 and 10 mm respectively.

Tests (1-8) (deformable situation) were experimentally performed in Abdul-Latif (2000), tests noted by (*) are experimentally conducted in this work (deformable and non-deformable situation)

3 Basic Equations

A numerical analysis capability provides a rational basis for estimation and expectation of the required force and energy during the plastic deformation process. An evaluation of the stress and strain history of the deformed solid makes it possible to identify the limitations of such process. This analysis leads to estimate, for example, the load-deflection characteristic and the dissipated energy at any deformed state of the deformed solid.
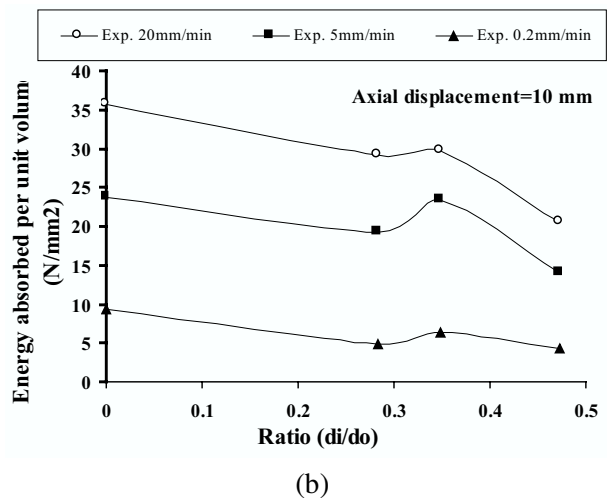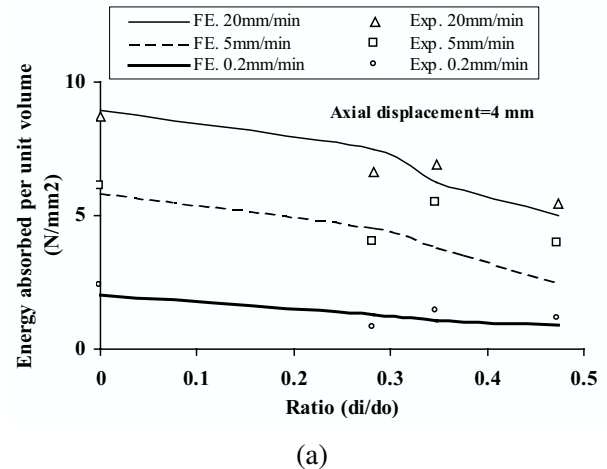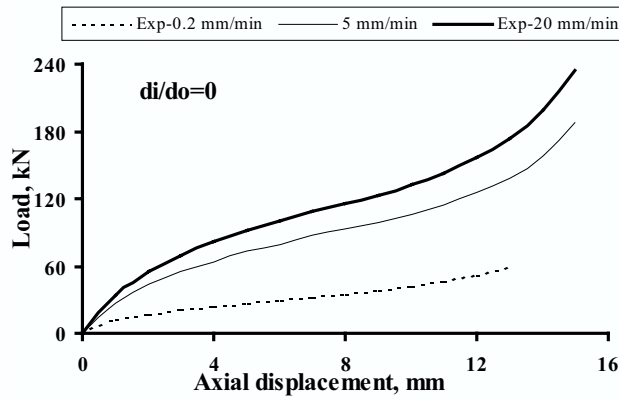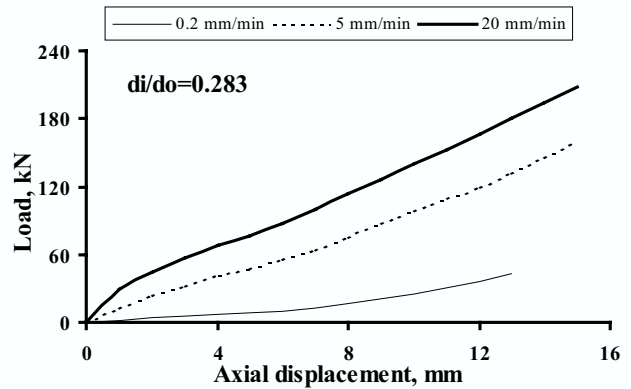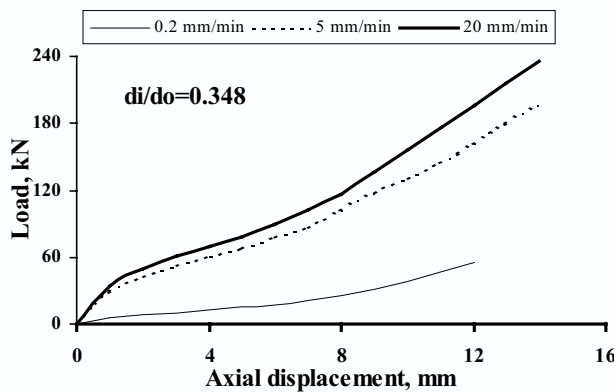

(a)

(b)

Figure 4 : Experimental and theoretical variations of energy absorbed per unit volume, with di/do ratio for the deformable and non-deformable situation at different strain rates for axial deflections: (a) δ=4 mm and (b) δ=10 mm.
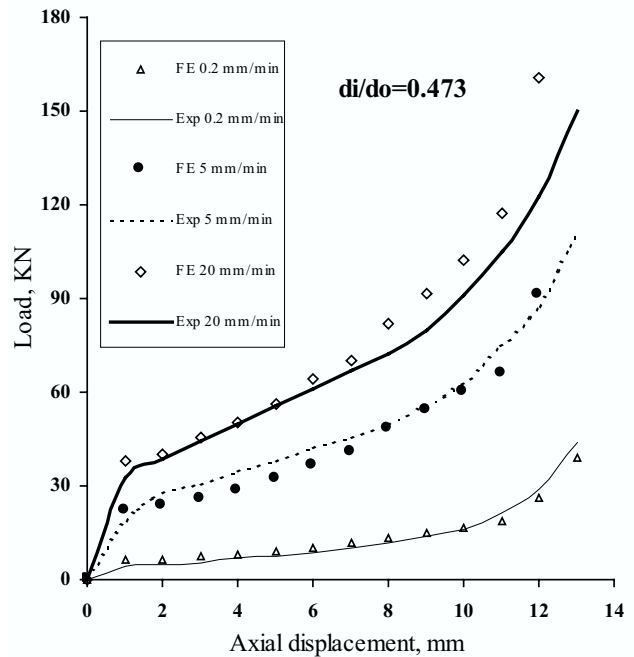
(a)

(b)

(c)

(d)

Figure 2 : Load-deflection characteristics at different strain rates in the deformable and non-deformable situation for the specimens of: (a) R=0, (b) R=0.283, (c) R=0.348, (d) R=0.473.

Table 1 : Dimensions of tested cylinders

No.	(do), mm	(di), mm	di/do (R)	length ℓ_o, mm	volume, mm³
*1	24.4	0.0	solid	120	56111.56
2	24.7	2.5	0.1	120	56910.57
*3	24.9	5.08	0.204	120	56002.37
*4	25.5	7.2	0.283	120	56398.81
5	25.7	7.71	0.3	120	56647.24
*6	26.1	9.1	0.348	120	56397.87
7	27.2	11.7	0.43	120	56826.69
*8	27.7	13.1	0.473	120	56141.51

In the present work, the idea is to assess the validity of the simulation of the lateral plastic collapse of two geometrically identical cylinders. Starting from the principle of virtual power (PVP), the boundary value problem of arbitrary amount of deformation is formulated in the deformed configuration. Its transformation and linearization result from the well-known incremental form of the updated Lagrangian formulation [Bathe, Ramm, and Wilson (1975); Cescotto, Frey and Fonder (1979) and Atluri (1980)]. Alternatively, a Total Lagrangean approach may be used [LeVan and LeGrognec(2001)]. To describe the material behavior, the Norton-Hoff's law is used. Despite the simplicity of its expression, such a law can take into account the sensitivity to strain rate representing a first acceptable approximation of numerical analysis conducted in this work. However, improvement of the numerical results can be performed by more sophisticated viscoplastic constitutive equations, which are generally presented as first order differential equations leading to numerical approximations given by the local numerical integration scheme. The incompressibility condition is satisfied through the introduction of a penalty term in the PVP. Finally, the resulting discrete equations are solved by Newton-Raphson algorithm in the presence of material and contact non linearities. Compressive forces and the energy absorbed during the plastic collapse are appropriately reproduced by the model. The general equations presented below give the finite element formulation of the structure problem based on the Norton-Hoff law. This latter, which is implemented in the commercial finite element code FORGE2, is well established and available in several references using this code [for example, Chenot (1992); Moal, Massoni and Chenot (1992); Shnizu, Soyris, Massonui, and Chenot (1992)].

3.1 Superplastic material: constitutive equation

The superplastic material is assumed to be homogeneous, isotropic and incompressible. The following condition either on the velocity filed $\mathbf{v}$ or on the strain rate tensor $\mathbf{D}$ $=\frac{1}{2}\left(\mathrm{grad}^{\mathrm{t}}(v)+\mathrm{grad}(v)\right)$ is added:

$$\mathrm{div}(v) = \mathrm{tr}(D) = 0 \tag{1}$$

The elastic strain is negligible with respect to the irreversible (inelastic) strain and has a little effect on the

material flow. The inelastic flow law of the Norton-Hoff type is often used in the following form:

$$\sigma = 2K((\sqrt{3\overline{d}})^{m-1}D \tag{2}$$

where σ is the Cauchy stress tensor which coincides with its deviatoric part, $\overline{d} = \sqrt{\frac{2}{3}(\mathbf{D:D})}$ the effective strain rate, K the material consistency and m the strain rate sensitivity index. The expression of the employed law involving large deformation, does not pose the problem of the material frame indifference. It has an objective form since it does not introduce stress rate.

3.2 Contact and friction equations

At the interfaces between the die and the part and between the accomodator and the part, $\partial_c\Omega$, the non-penetration condition is given by:

$$(\mathbf{v} - \mathbf{v}_{\mathrm{die}}).\mathbf{n} = \mathbf{v}_s.\mathbf{n} = 0 \tag{3}$$

where $\mathbf{v}_{\mathrm{die}}$ is the die velocity and $\mathbf{n}$ the normal to the die. With neglecting the reversible friction displacement, a viscoplastic friction behavior can be used. It is described by a non-linear relation between the shear stress $\tau = \sigma\mathbf{n}.\mathbf{t}$ ($\mathbf{t}$ is the tangent to the die surface) and the tangential velocity difference $\mathbf{v}_s$ at the die-part interface $\partial_c\Omega$:

$$\tau = -\alpha_f K|\mathbf{v}_s|^{q-1}\mathbf{v}_s \tag{4}$$

where α_f is the friction coefficient and q (which is often equal to m) being the sensitivity index to the sliding velocity.

3.3 Integral formulation

The finite element analysis necessitates the description of the boundary value problem associated to the collapse of the identical cylinders. The domain of the deformed solid is denoted by Ω and the equilibrium equation is:

$$\mathrm{div}(\sigma) + \rho\mathbf{f} = 0 \tag{5}$$

where ρs the material density, $\mathbf{f}$ the body force vector (generally the gravity force). The boundary conditions (Fig. 5) correspond to:

- the free surface $\partial_f\Omega$

$$\mathbf{T} = \sigma\mathbf{n} \tag{6}$$

- the die-part and the accomodator-part interfaces $\partial_c\Omega$, where the friction law (4) and the non-penetration condition (3), are imposed.
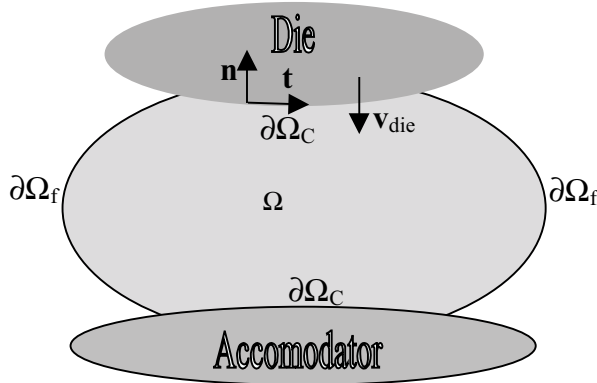

Figure 5 : Boundary value problem

As an alternative to the local formulation represented by the relations (5) and (6), the PVP is suitable for NLFE method application. Accordingly, the PVP gives the integral form, which holds for any virtual velocity field $\mathbf{v}^*$

$$\int_\Omega \sigma : \mathbf{D}^* dV + \int_\Omega \rho\mathbf{f}\mathbf{v}^* dV - \int_{\partial_c\Omega} \tau\mathbf{v}^* dS = 0 \tag{7}$$

with condition (3) again and $\mathbf{D}^*$ is the virtual strain rate. For Norton-Hoff incompressible materials, the penalty formulation is often used. For any virtual velocity field $\mathbf{v}^*$, the PVP becomes:

$$\int_\Omega \sigma : \mathbf{D}^* dV + \int_\Omega \rho\mathbf{f}\mathbf{v}^* dV - \int_{\partial_c\Omega} \tau\mathbf{v}^* dS$$
$$+ \int_\Omega \rho_p \text{div}(\mathbf{v})\text{div}(\mathbf{v}^*) dV = 0 \tag{8}$$

where $\rho_p(\cong 10^5 - 10^7)$ is a penalty coefficient. Moreover, the total dissipated energy of the deformation process at the time t is determined using the following expression in the case of the Norton-Hoff's friction law:

$$\mathbf{w} = \int_{t_0}^{t} \left[\int_\Omega K(\sqrt{3d})^{m+1} dV - \int_{\partial_c\Omega} \alpha_f K |\mathbf{v}_s|^{q+1} dS \right] dt \tag{9}$$

3.4 Space and time discretisation

Using an updated Lagrangian method, the process to be simulated is divided into small time steps on which the mechanical problem is solved. Introducing the usual finite element interpolation [Zienkiewicz (1977)], the velocity vector $\mathbf{v}$ at any point within the element can be expressed in terms of the nodal velocities $\mathbf{V}_n$ and the interpolation functions $\mathbf{N}_n$:

$$\mathbf{v} = \sum_n \mathbf{N}_n(\xi)\mathbf{V}_n \tag{10}$$

ξ are the local coordinates which allow to define the isoparametric element in term of the vectors of nodal coordinates $\mathbf{X}_n$ by:

$$\mathbf{x} = \sum_n \mathbf{N}_n(\xi)\mathbf{X}_n \tag{11}$$

Similarly, the strain rate is expressed in terms of the nodal velocities and the classical operator $\mathbf{B}_n$ (shape functions gradients)

$$\mathbf{D} = \sum_n \mathbf{B}_n\mathbf{V}_n \tag{12}$$

Substituting (2), (10) and (11) into (8), the finite element discretizing procedure leads to the following expression of the PVP:

$$\int_{\Omega_t} 2K(\sqrt{3d})^{m-1}\mathbf{D} : \mathbf{B}_n dV + \int_{\Omega_t} \rho\mathbf{f}\mathbf{N}_n dV \tag{13}$$
$$- \int_{\partial_c\Omega_t} \alpha_f K |\mathbf{v}_s|^{q-1}\mathbf{v}_s\mathbf{N}_n dS + \int_{\Omega_t} \rho_p \text{div}(\mathbf{v})\text{tr}(\mathbf{B}_n) dV = 0$$

Equation (13) together with the constraint (3) imposed by the evolving contact condition are iteratively solved by the Newton-Raphson algorithm summarized as follows:

(i) as a first trial, the solution of (13) is generally obtained with the linear behavior (i.e. m=p=1).

(ii) let $\mathbf{V}^{(k-1)}$ the velocity at iteration (k-1). For the iteration (k), the velocity field is updated using

$$\mathbf{V}^{(k)} = \mathbf{V}^{(k-1)} + \Delta\mathbf{V}^{(k)} \tag{14}$$

and the non linear discrete equation (13), which can be written in the compact form $\mathbf{R}(\mathbf{V}) = 0$, is linearized according to

$$\mathbf{R}(\mathbf{V}^{(k)}) = \mathbf{R}(\mathbf{V}^{(k-1)}) + \frac{\partial\mathbf{R}}{\partial\mathbf{V}}(\mathbf{V}^{(k-1)})\Delta\mathbf{V}^{(k)} = 0 \tag{15}$$

which allows to compute $\Delta\mathbf{V}^{(k)}$ by solving a linear system if the tangent stiffness matrix $\mathbf{K_T}^{(k)} = \frac{\partial\mathbf{R}}{\partial\mathbf{V}}(\mathbf{V}^{(k-1)})$ is not singular.

(iii) a sub-incrementation procedure may be necessary to speed up the numerical process, or even to achieve convergence. In that case, equation (14) is rewritten as:

$$\mathbf{V}^{(k)} = \mathbf{V}^{(k-1)} + \gamma\Delta\mathbf{V}^{(k)} \tag{16}$$

starting with $\gamma = 1$, it is divided by 2 until:

$$\left|\mathbf{R}(\mathbf{V}^{(k)}(\gamma))\right| \leq \left|\mathbf{R}(\mathbf{V}^{(k-1)}(\gamma))\right| \tag{17}$$

Finally, the steps (i) and (ii) are repeated until a given accuracy is reached.

The resolution of the non-steady problem can be easily pursued by using an explicit scheme to update the new configuration. If the domain at time t is Ω_t , the coordinates, in the new configuration $\Omega_{t+\Delta t}$, are updated by writing:

$$\mathbf{X}_{t+\Delta t} = \mathbf{X}_t + \mathbf{V}(t)\Delta t \tag{18}$$

3.5 Related topics

Evolving contact: In the framework of the explicit integration scheme, the iterative contact algorithm is demonstrated as follows. The surface of the die which is assumed at rest for simplicity is described by a function g

such that g(x)¿0 corresponds to the inside of the die. If at time t a node number n, with vector coordinates $\mathbf{X}_n^t$, is on the free surface, i.e. if $g(\mathbf{X}_n^t) < 0$, the onset of contact is characterized by:

$$g(\mathbf{X}_n^t + \Delta t\mathbf{V}_n^t) \leq 0 \tag{19}$$

When the node penetrates into the die during the time interval Δt then, it is projected back on the die surface at time t+Δt. In order to minimize the volume variations due to this projection, the time step length can be adjusted in such a way that the new node that comes in contact do not penetrate into the die, but it may increase significantly the number of time steps.

Now, if at time t the node is already in contact with the die, two cases have to be considered: (i) the normal stress is compressive at time t and the node n remains therefore in contact. But, if the tool is not planar in the vicinity of the node n, a reprojection on the die will be again necessary; (ii) the normal stress is no longer compressive, the point is then allowed to loose its contact with the die.

Remeshing: with an updated Lagrangian formulation, the nodes of the mesh follow the kinematic evolution of the material points. This method leads to a highly distorted mesh due to the large deformation of the material. Moreover, when the final topology is very different from the initial one, the same mesh topology is generally not convenient for the whole process. For these reasons, remeshing is mandatory, and takes place frequently in some examples (it can be more than 300). Therefore, a new mesh is automatically generated as soon as one of the following criteria is reached: (i) distortion of a finite element or a segment of the boundary; (ii) bad description of the die-part interface; (iii) large curvature of the segments of the free boundary and finally (iv) detection of a fold. For example, in the case where a fold is detected, the overlapping part of the domain is then removed from the boundary description before the mesh regeneration (Fig. 6). This leads to some volume losses, but this simple procedure makes the simulation possible to continue. Moreover, this procedure allows, in this study, to model the contact between two deformable cylinders showing satisfactory results.
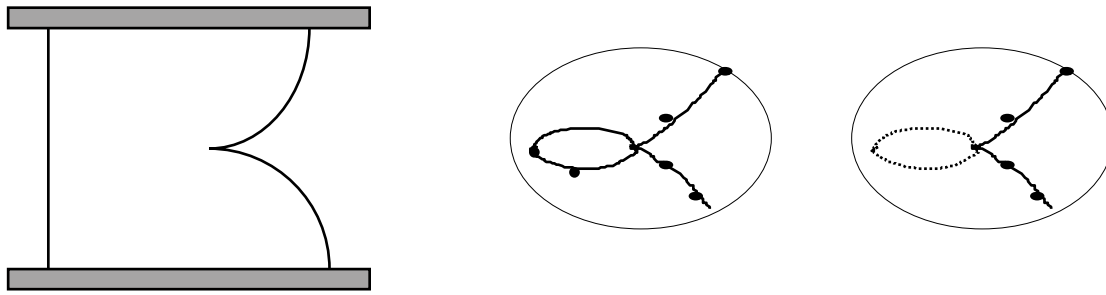
Figure 6 : Folding defect noticed by the remeshing procedure when two boundary segments cross each other, elimination of the folded area by the remeshing procedure

4 Discussion

4.1 Experimental results: case of deformable/non-deformable cylinders

Let us now discuss the different experimental results carried out for determining the effects of specimen geometry and the strain rate on the energy absorption for all mentioned cases of DND situation (Table 1).

The representative plastic strain rate was already estimated [Abdul-Latif (2000)] during the lateral collapse. In fact, under a constant compressive loading, when the axial deflection (δ) has a small value, the corresponding strain rate has relatively a quite high value. This is due to the fact that, for such complicated structure, the plastic strain begins to locally evolve in a rapid rate even under quasi-static loading. Progressively, the greater the axial displacement, the greater the indentation process (indentation of the non-deformed cylinder in the deformed one) that takes place, the lower becomes the strain rate, its value continues thus to gradually decrease with increasing the axial deflection up to stabilized value. According to Abdul-Latif (2000), the representative strain rates ($\dot{\varepsilon}$) are 7×10^{-5}/s, 1.8×10^{-3}/s and 7×10^{-3}/s corresponding the cross head speeds, 0.2, 5 and 20 mm/min, respectively. For further details about the representative strain rate determination, the reader can see the above reference.

Figs. 2a, b, c and d display that whatever R and $\dot{\varepsilon}$ values, there are three phases of force evolution during the plastic collapse. This evolution is more obvious in the cases of R=0 and R=0.473; first, for a small axial deflection, the compressive force evolves rapidly with δ. Then, in the second phase, the evolution slows down for certain range of δ due to the equilibrium between the increas-

ing of the indentation process and the relative decreasing of the strain rate. Contrary to the second phase, the force evolves rapidly with δ in the final phase. In fact, the strain rate reaches practically its steady state for a relatively high value of δ, while the non-deformable cylinder continues to penetrate into the deformable cylinder leading to a large area of contact. Hence, high frictional stresses give rise to a sudden change in required force. Whatever the value of R, this behavior is clearly observed at the highest strain rate (7×10^{-3}/s). Examination of Figs. 2a, b, c and d reveals that the load-deflection curves, plotted at different strain rates, indicate the increasing of the compressive force whenever the strain rate is increased for a given deflection. The curves diverge with increasing deflection due to the change in the strain rate reflecting the material sensitivity to strain rate. In addition, the deflection increases with an increase in the R ratio, for example, at a load of 50 kN, the deflections in the specimens of R of 0, 0.283, 0.348 and 0.473 are respectively 1.4 , 2, 1.8 and 3.4 mm at a representative strain rate of 7×10^{-3}/s, while the deflections of 2.4, 5, 2.2 and 7.4 mm result at a strain rate of 1.8×10^{-3}/s. In conclusion, at any particular load, the deformation increases as the R ratio is increased. Similarly, as the strain rate increases, the required load is also increased at any particular deflection.

As far as the variation of the energy absorbed per unit volume with R is concerned, it is recorded for two axial deflections of 4 and 10 mm (Fig. 4) that the geometrical factor (R) has a significant effect on the energy absorption for a given axial deflection and strain rate. This figure also shows that the relationship between the energy absorbed per unit volume and R ratio at different strain rates (1.8×10^{-3}/s and 7×10^{-3}/s) is relatively of a similar pattern. However, this behavior changes at a strain rate of

7×10^{-5}/s, notably for R$\geq$ 0.348, and the absorbed energy becomes less steep with respect to other strain rates. This is due to the fact that the superplastic material is more sensitive to strain rate at a range of 10^{-4}/s to 10^{-3}/s. This behavior is in agreement with a previous result recorded by Al-Naib & Duncan (1970). Moreover, it is obvious from examination of Fig. 4 that the mechanical behavior of the cylinder of R=0.348 changes due to the change of the flow mechanism.

The flow mechanism around the cylinder bore of the deformable specimen of R=0.348, as an example, is studied under strain rate of 1.8×10^{-3}/s at two selected axial deflections of 6 and 10 mm (Fig. 3). In the first case (δ=6 mm), the bore is highly deformed and its closure does not completely occur, while at 10 mm of deflection, the bore closure is completely terminated. It is important to note that the difference between the real section and the predicted one is due to the hypothesis of plane strain adopted by the finite element modeling, while the experimental plastic flow takes place in three dimensions. Thus, it is obvious that the cross-sectional area of the real deformed cylinder is smaller than that of predicted one.

To investigate the strain rate effects on the bore closure for a such material, seven cross head speeds (0.2, 0.5, 1, 2, 5, 10 and 20 mm/min) are used giving representative strain rates 7×10^{-5}/s, 1.8×10^{-4}/s, 4×10^{-4}/s, 7×10^{-4}/s, 1.8×10^{-3}/s, 4×10^{-3}/s and 7×10^{-3}/s, respectively. Under each strain rate, the cylindrical specimen of di/do=0.473 is loaded up to 10 mm of axial deflection. Then, the width of cavity is measured by a profile projector at a magnification of ten. Fig. 7 points out that the greater the strain rate, the more the increasing of the cavity width takes place up to a strain rate of 4×10^{-4}/s. After that, such a width decreases with the strain rate increasing. Hence, this mechanical behavior confirms the material sensitivity to strain rate in the range of 10^{-4}/s to 10^{-3}/s notably at 4×10^{-4}/s.

4.2 Experimental results:
Case of deformable/deformable cylinders

First of all, it is important to note that some typical experimental results concerning this case are extracted from Abdul-Latif (2000). All the experimental results related to deformable/deformable case are performed using several constant compressive cross head speeds (0.2, 0.5, 2 and 10 mm/min) and different geometries of cylinder (Table 1). According to Abdul-Latif (2000), the material
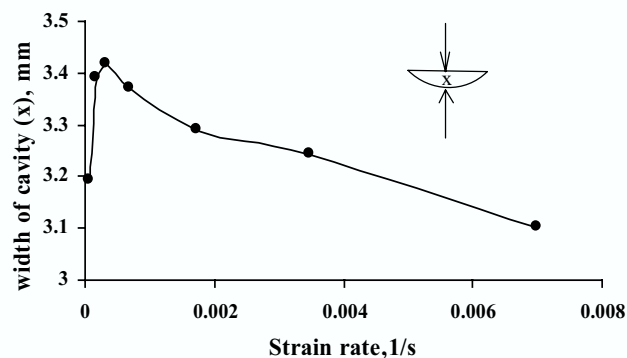
Figure 7 : A plot showing the variation of width of the cavity, with strain rate of the hollow cylinder of di/do=0.473 for an axial deflection of 10 mm in the deformable and non-deformable situation.

consistency (K) and the strain rate sensitivity (m) have been calibrated giving respectively 180 MPa and 0.395. An examination of Fig. 9 reveals that the load-deflection curve plotted at different strain rates, indicates that the required force increases whenever the strain rate is increased for a given deflection. On the other hand, since the utilized material is sensitive to the strain rate, thus, the curves diverge with increasing deflection due to the change in the strain rate. In addition, the deflection increases with an increase in the strain rate. For example, at a load of 30 kN, the deflections in the specimens of R of 0.3 is 2 mm at a representative strain rate of 3.5×10^{-3}/s, while the deflection of 6 mm results at a strain rate of 7×10^{-4}/s and 9.5 mm at a strain rate of 1.8×10^{-4}/s. In conclusion, at any particular load, as the strain rate increases, the related deflection is decreased.

The variation of the energy absorbed per unit volume with R is now examined. Fig. 10 shows, for an axial deflections of 8 mm for four strain rates, that the factor R has a significant effect on the energy absorption for a given strain rate. Moreover, the evolution of the energy absorbed per unit volume with R ratio at strain rate of 7×10^{-5}/s and 1.8×10^{-4}/s is of a relatively similar pattern. whereas, this behavior starts to change at a strain rate of 7×10^{-4}/s, in which the effect of changing R on the absorbed energy is more steep, while at a strain rate of 3.5×10^{-3}/s the change becomes sharper, and this is due to the fact that the superplastic materials are more sensitive to strain rate at a range of 10^{-4}/s to 10^{-3}/s as it has been shown in Al-Naib and Duncan (1970).

4.3 Numerical results:
Case of deformable/deformable cylinders

Several compression tests of the identical pair of cylinders were predicted using the commercial finite element code FORGE2 in order to study their lateral collapse and to compare the material behavior predictions with the experimental results.

This structure exhibits many important features such as: (i) non-homogeneous deformations, (ii) variable regions of contact between deformed cylinders and rig, (iii) the varying strain rates at material points, and (iv) rapid rise of total rig force when an important part between the two cylinders is in contact.

For the finite element analysis, the rig is modeled as a translating rigid surface. The identical pair of cylinders are intensively deformed at the tangential region (free deformation region between the two cylinders (outer cylinder halves)). The geometry of the undeformed mesh of the cylinders is shown in fig. 8 assuming that there is one plane of symmetry. Accordingly, only one half
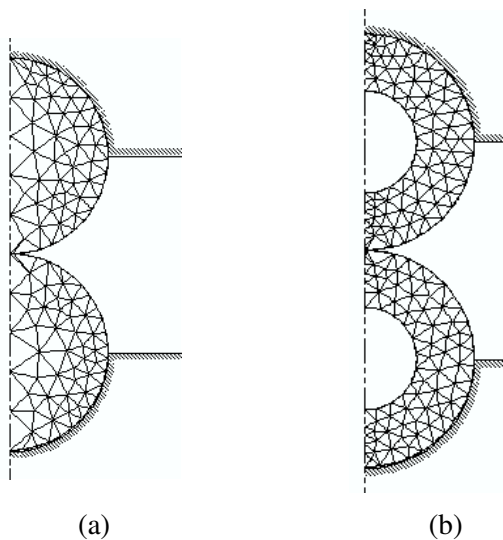

(a)   (b)

Figure 8 : Finite element mesh: (a) for solid cylindrical specimens, (b) for hollow cylindrical specimens of R=0.473.

of the specimen is modeled with a six-noded triangular plane strain element. The number of elements used was generally 299-392 and the number of calculations steps was 267-346. A number of remeshings has to be performed automatically because of severe mesh distortions occurring at the tangential region for the solid cylinders producing flattening and around the bore for the hollow

ones. In addition, the fold detected at the contact between the two cylinders increases the relative density values of meshes to 68-87 in order to remove the overlapping part. Moreover, the friction between the specimen and the die is not experimentally characterized. However, repeated simulations with different friction coefficient values give no significant difference on the obtained load-deflection curves. The rest of simulations are then performed in the frictionless case.

Many aspects are going to be investigated in this finite element simulation. In fact, under quasi-static loading conditions, the material exhibits strain rate sensitivity. It can be noted from examination of Fig. 9, for di/do=0.3, that the load-deflection curves (plotted at different strain rates) indicate that the required force increases whenever the strain rate is increased for a given deflection. The experimental results are included in the figure for comparison and show a good agreement with predictions. Note that jumps in rig force occur in the predicted result whenever new nodes came in contact with the rig. Further, the predictions describe well the material sensitivity to the strain rate.

Generally, at any corresponding deflection and R ratio, it is obvious also that there is a sudden change in the amount of the energy absorbed per unit volume as the strain rate is increased. This is based on the sensitivity of the used material to the change rate. Fig. 10 shows a correct description of the finite element model comparing to the experimental result. For the energy absorbed, it is recorded, as an example, for an axial deflection of 8 mm (Fig. 10) that (R) has a significant effect on the energy absorption for a given axial deflection and strain rate. Such behavior is in agreement with the experimental results.

Fig. 11a and Fig. 12a point respectively out the deformed finite element mesh of the solid specimen after 10 mm and hollow specimen (R=0.473) after 13 mm of axial deflection. It is clearly displayed, in the case of R=0, that the high distortion of the mesh is developed at the tangential region of cylinders, whereas the two semi-cylindrical parts, constrained by specimen accomodator, remain practically without any deformation effect. On the other hand, for the hollow case (R=0.473), a high distortion of the mesh is observed around the bore, but the parts under the accomodator remain intact.

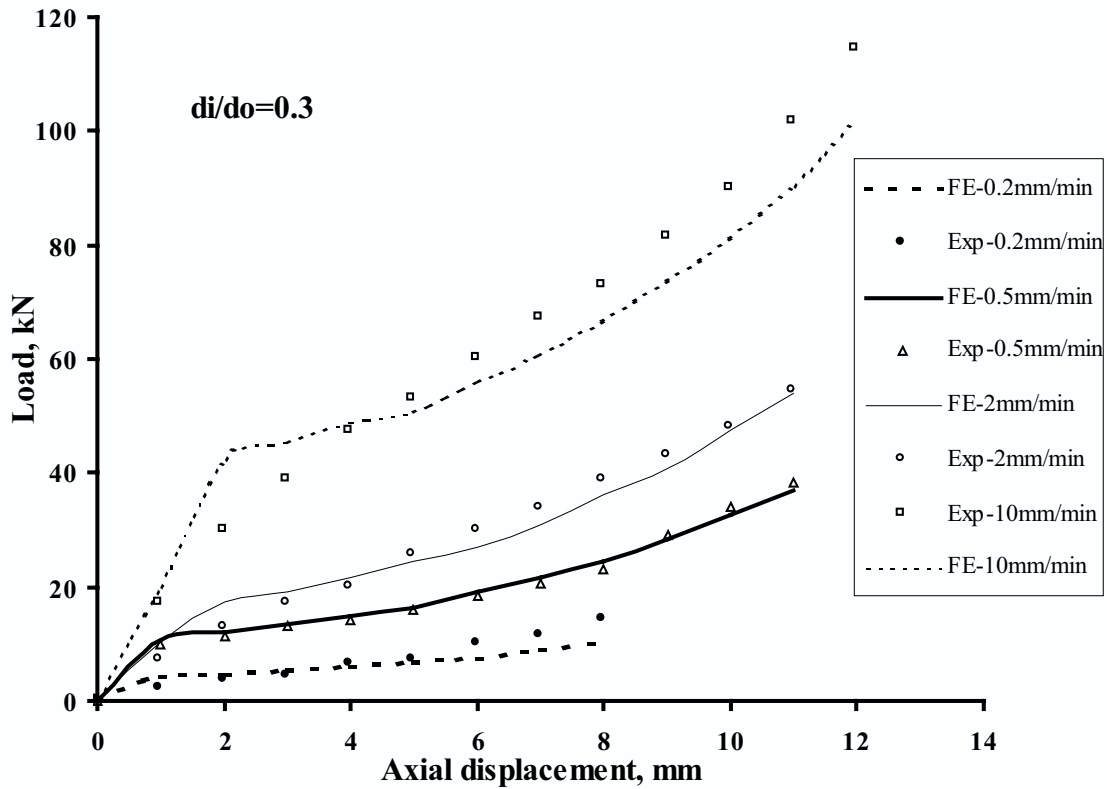In order to predict the mode of deformation in the tangential region between the two identical cylinders, the distri-

Figure 9 : Experimental and theoretical load-deflection characteristics at different strain rates in the deformable situation for the cylindrical specimens of R=0.3.
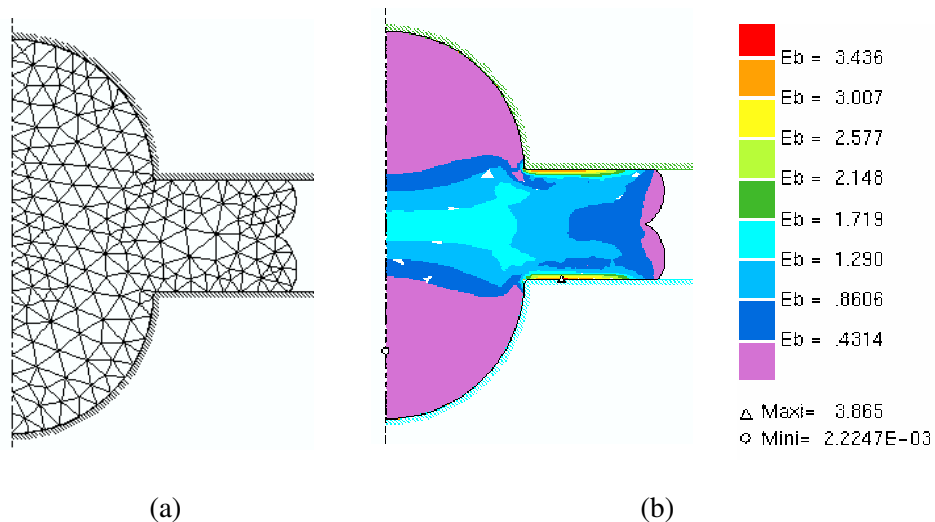

(a)   (b)

Figure 11 : Finite element plastic collapse simulation for the deformable situation in the case of solid specimens: (a) finite element mesh, (b) plastic strain distribution inside the deformed specimens after 10 mm axial deflection.
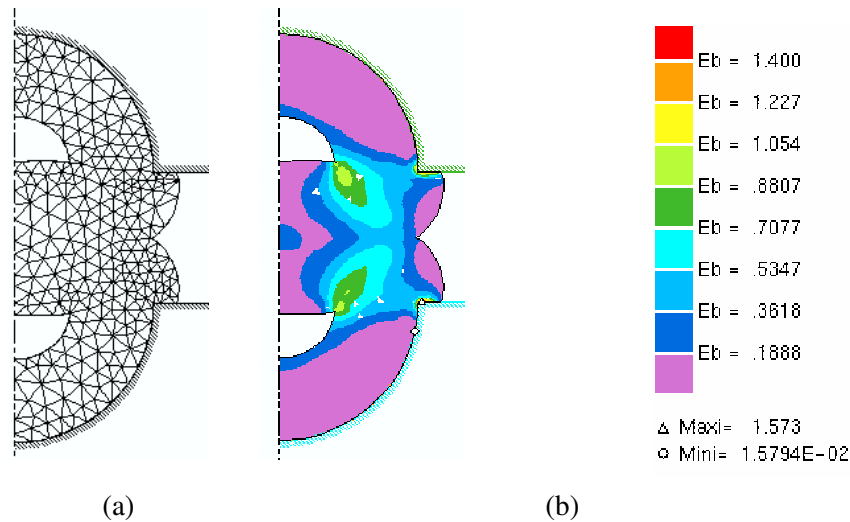
(a)   (b)

Figure 12 : Finite element plastic collapse simulation for the deformable situation in the case of hollow specimens (R=0.473): (a) finite element mesh, (b) plastic strain distribution inside the hollow deformed specimen after 13 mm axial deflection.
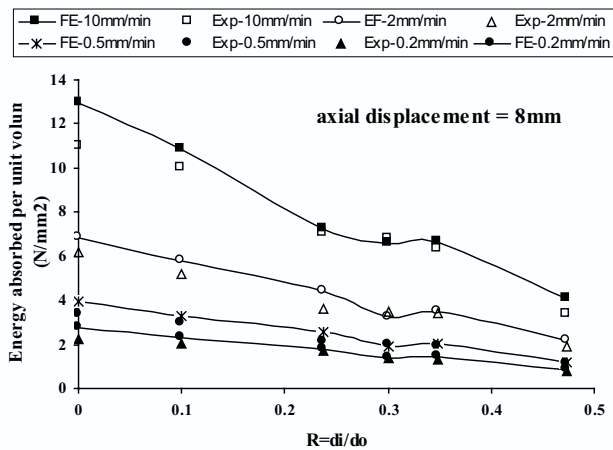

Figure 10 : Comparison between the experimental and theoretical variations of energy absorbed per unit volume, with di/do ratio for the deformable situation at different strain rates for an axial deflection of 8 mm.

bution of the plastic strain is presented in Fig. 11b and Fig. 12b for the solid and hollow cylinders. It is shown that the flow mechanism is different for these cylinders. In fact, for the solid specimen, a zone of intense plastic flow is observed in the flattened region during the compressive loading. Moreover, a 'dead zone' with less plastic strain is pointed out in the two semi-cylindrical parts under the accomodator. For the hollow specimen, the two semi-cylindrical parts under the accomodator suffer from a more important plastic strain than that in the first case. However, its intensity remains distinctly lower than that in the tangential region and around the bore. In fact, the flow mechanism which develops towards the bore direction undergoes plastic strain localizations as plastic hinges in the lateral extremities of the deformed bore (fig. 12). These plastic hinges are often observed in the crushing of the thin tube cases. These results are in a good agreement with experimental observations recorded by Abdul-Latif (2000).

4.4 Numerical results: ## *Case of deformable/non-deformable cylinders*

Four geometries of different values of R (0, 0.283, 0.348, 0.473) are chosen for the numerical investigations. The material properties used here are the same as in the previous problem. The geometry of the rig is transformed to replace the upper deformed cylinder and becomes as a translating rigid surface. The finite element data adopted for the calculation is the same as in the above case.

Fig 13 shows the finite element mesh for the specimens with R = 0 and 0.348 where the initial mesh contains respectively 292 and 290 six-noded triangular plane strain elements. Symmetry in the problem allows to use a half part of the cylinder. The relative density values of meshes are 44-62.
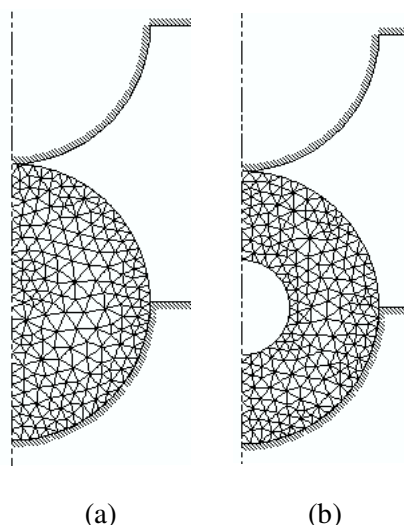

(a)   (b)

Figure 13 : Finite element mesh for the deformable and non-deformable situation: (a) for the solid cylindrical specimen, (b) for the hollow cylindrical specimen of R=0.348.

The deformed mesh of the cylinder with R=0.348 is presented in Fig. 14b. As an average, 5 iterations per increment are required in this computation to obtain the converged solution. After a deflection of 6 mm, the deformed cylinder has acquired a shape which agrees quite well with the experimental one (Fig. 3). Referring to the deformed mesh, the elements in lateral bore region are highly distorted leading to plastic strain localization zones (plastic hinges). It is obvious from this region that the element becomes severely distorted and leads to increasing the frequency of remeshing operation. Moreover, the experimental and predicted load-deflection curves are shown in Fig. 2a, 2b, 2c and 2d at three compressive strain rates. The effect of the strain rate on the mechanical behavior of this structure during the plastic collapse is appropriately described by the modeling.

For any given deflection and R ratio, one observes that there is a change in the amount of the energy absorbed per unit volume as the strain rate is increased. This is based on the sensitivity of the used material to the strain
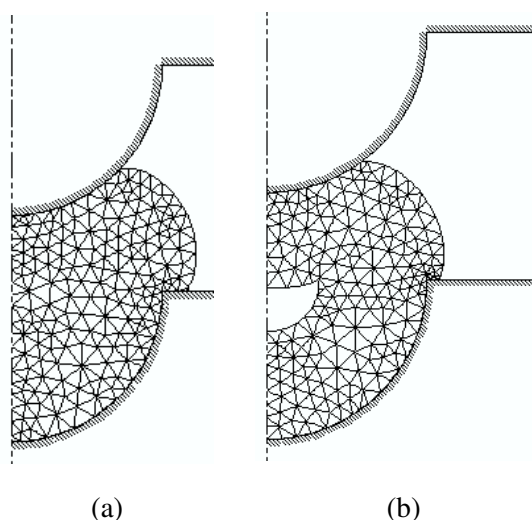

(a)   (b)

Figure 14 : Finite element plastic collapse simulation for the deformable and non-deformable situation: (a) deformed finite element mesh after 5 mm axial deflection for a solid specimen, (b) deformed finite element mesh after 6 mm axial deflection for a hollow specimen (R=0.348).

rate change. Fig. 4a points appropriately out a description of the finite element model comparing to the experimental result. The variation of the energy absorbed per unit volume is recorded for an axial deflection of 4 mm (Fig. 4), as an example, at the three rates of strain. The factor (R) has a significant effect on the energy absorption for a given axial deflection and strain rate.

As it was previously shown in Fig. 7 for R=0.348 and δ=6 mm, the bore is not completely closed and at 10 mm the bore closure is completely terminated. This figure displays that the NLFE method describes fairly well this mode of deformation under these conditions.

5   Conclusions

The superplastic tin-lead alloy can be used at a strain rate ranging from 10^{-5}/s to 10^{-3}/s to represent the behavior of metallic materials in the intermediate and high strain rates 1/s to 10^4/s.

The non-linear finite element method represents a useful device to simulate the effect of the strain rate and the cylindrical geometries on the plastic collapse behavior in the cases of deformable situation and deformable and non-deformable one. With this modeling, the flow mechanism of cylinders during the lateral plastic collapse (for

both situations) is successfully reproduced and compared with some available experimental observations.

The used Norton-Hoff's law describes well the plastic behavior of superplastic tin-lead alloy and its sensitivity to the strain rate in the range of 10^{-5}/s to 10^{-3}/s, in spite of its very simple form. However, it will be a judicious choice when a more sophisticated viscoplastic constitutive law will be employed in order to improve predicted results.

The capability of the two systems (deformable and deformable and non-deformable situations) to absorb the energy increases first with an increase in the strain rate and secondly with a decrease in the ratio R for the same volume and cross-sectional area. Under the same load and strain rate, the amount of deflection in the specimen decreases with the decrease in the R ratio.

References

Abdul-Latif, A. (2000): On the Lateral Collapse of an Identical Pair of Cylinders. Int. J. Solids Struct., vol. 37, pp. 1955-1973.

Al-Naib, T. Y. M.; Duncan, J. L. (1970): Superplastic metal forming. Int. J. Mech. Sci., vol. 12, pp. 463-477.

Atluri, S.N. (1979): On rate principles for finite strain analysis of elastic and inelastic nonlinear solids. in: Recent Research on Mechanical Behavior of solids, Univ of Tokyo press, pp. 79-107.

Bathe, K.J; Ramm, E.; Wilson, E.L., (1974): Finite element formulations for large deformations dynamic analysis. Int. J. Num. Meths. Engrg, vol. 9, pp. 353-386.

Cescotto, S.; Frey, F.; Fonder, G. (1979): Total and updated Lagrangian descriptions in nonlinear structural analysis. A unified approach, in R. Golwinski, ed., Energy Methods in Finite Element Analysis (Wiley, new York), pp. 203-296 .

Cheng, J. H.; Kikuchi, N. (1985): An Analysis of Metal Forming Processes Using Large Deformation Elastic-Plastic Formulations. Comp. Meth. Appl. Mech. Engng., vol. 49, pp. 71-108.

Chenot, J. L.; Wood, R. D.; Zienkiewicz O. C. (eds) (1992): Proc. of Numerical Methods in the trial Forming Process. NUMIFORM 92. Valbonne, France, 14-18 September.

Chenot, J. L. (1992): Finite Element Modeling of metal forming: Recent Achievement and Future challenges. Proceeding of the Third International Conference on Computational Plasticity, DRJ Owen, E. Onate & E. Hinton Eds., Pineridge Press.

DeRutz, J. A.; Hodge, JR. (1963): Crushing of a Tube between Rigid Plates. J. Appl. Mech., vol. 30, pp. 391-395.

Ezra, A. A.; Fay, R. J. (1970): An Assessment of Energy Absorbing devices for Prospective Use in Aircraft Impact Situations. Dynamic Response of Structures. G. Hermann and N. Perrone Eds., Pergamon Press.

Hibbitt, H. D. (1979): Some Flower Forces and Load Stiffness. Inter. J. Numer. Meths. Engrg. vol. 14, pp. 217-232.

Johnson, W. (1972): Impact strength of materials. London: Edward Arnold, London.

Johnson, W.; Mellor, P. B. (1975): Engineering Plasticity. Van Nostrand, London, UK.

Johnson, W.; Reid, S. R.; Reddy, T. Y. (1977): The Compression of Crossed Layers of Thin **Johnson, W.; Reid, S. R.** (1978): Metallic Energy Dissipating Systems. Rev. vol. 31, pp. 277-288.

Johnson, W.; Reid, S. R. (1986): Metallic Energy Dissipating Systems. Rev. vol. 31, pp. 277-288; Appl. Mech. Update 1986, pp. 315-319.

Jones, N. (1989): Structural Impact. Cambridge Press, Cambridge, UK.

LeVan, A.; LeGrognec,P. (2001): Modeling and Numerical Computation of Necking in Round Bars Using a Total Lagrangian Elastoplastic Formulation. CMES: Computer Modeling in Engineering & Sciences, vol. 2, no. 1, pp 63-72.

McMeeking, R. M.; Rice, J. R. (1975): Finite Element Formulations for Problems of Large Elastic-Plastic Deformation, inter. J. Solids Structures, vol. 11, pp. 601-616.

Tubes," Int. J. Mech. Sci., vol. 19, pp. 423-437.

Moal, A.; Massoni, E.; Chenot, J.L. (1992): Finite Element Modeling for the inertia welding process, Proceeding of the Third International Conference on Computational Plasticity, D.R.J. Owen, E. Onate & E. Hinton Eds., Pineridge Press.

Rawlings, B. (1974): Response of Structures to Dynamic Loads. Proc. Conf. On Mechanical Properties of Materials at High Rates of Strain, 279-298, Institute

of Physics Conference.

Reddy, T. Y.; Reid, S. R. (1979): Lateral Compression of Tubes and Tube-Systems with Side Constraints. Int. J. Mech. Sci., vol. 21, pp. 187-199.

Reid, S. R. and Reddy, T. Y. (1978): Effect of Strain Hardening on the Lateral Compression of Tubes between Rigid Plates. Int. J. Solids Structures, vol. 14, pp. 213-225.

Reid, S. R.; Reddy, T. Y. (1979): Effect of Strain Rate on the Dynamic Lateral Compression of Tubes. Proc. Conf. On Mechanical Properties of Materials at High Rates of Strain, pp. 288-298, Institute of Physics Conference, Oxford.

Rewood, R. G. "Discussion of ref. (DeRutz & Hodge (1963))" (1964): J. Appl. Mech., vol. 31, pp. 357-358.

Oden, J. T.; Kikuchi, N. (1982): Finite Element Methods for Constrained Problems in Elasticity," Int. J. Num. Meth. Engng, vol.18, pp. 701-25.

Oden, J. T.; Carey, G. F. (1984): Finite Elements Vol. V. Special Problems in Solid Mechanics. Prentice-Hall, Englewood Cliffs, New Jersey.

Pasquinelli, G. (1995): Simulation of Metal-Forming Processes By The Finite Element Method. Int. J. of Plasticity, vol. 11, pp. 623-651.

Shnizu, T.; Soyris, N.; Massonui, E.; Chenot, J.L. (1992): Development of a 3D code for the simulation of the Deep Drawing process. Proceeding of the Third International Conference on Computational Plasticity, D.R.J. Owen, E. Onate & E. Hinton Eds., Pineridge Press.

Signiorini, A. (1959): Questioni di Elastostatica Linearizzata e Semilinearizzata. Rend. di Matem. e delle Sur. Appl. 18.

Zaid, A. I. O.; Harding, J. (1974): Strain rate Effect in 1.5% Cr Mo Steel," University of Oxford, UK.

Zienkiewicz, O. C. (1977): The finite Element Method. McGraw-Hill, New York.